Electron-spin-echo envelope-modulation study of the distance between dangling bonds and hydrogen atoms in hydrogenated amorphous silicon

J. Isoya
University of Library and Information Science, 1-2 Kasuga, Tsukuba City, Ibaraki 305, Japan

S. Yamasaki, H. Okushi, A. Matsuda, and K. Tanaka
Electrotechnical Laboratory, 1-1-4 Umezono, Tsukuba City, Ibaraki 305, Japan
(Received 15 July 1992; revised manuscript received 20 October 1992)

Using the electron-spin-echo envelope-modulation method of pulsed electron spin resonance (ESR) technique, the spatial distribution of deuterium (chemically equivalent to hydrogen) nearby dangling-bond defects ($g=2.0055$) in deuterated amorphous silicon was investigated before and after light soaking. It is found, for both native and photocreated defects that the dangling bond is formed in the hydrogen-depleted region, being separated from the closest hydrogen atom by a distance of 4.2 Å (4.8 Å in the case of two closest hydrogen atoms), as estimated by using the point-dipole approximation. In both of two ESR signals ($g=2.004$, 2.013) under illumination (LESR), modulation is weaker than that of dangling bonds ($g=2.0055$), indicating a larger distance (4.8 Å to the closest hydrogen atom or 5.3 Å to the two closest hydrogen atoms by use of the point-dipole approximation). Defect-creation models, which have been proposed to explain the photoinduced metastability, are examined at a microscopic level.

I. INTRODUCTION

Introduction of hydrogen into amorphous silicon can drastically reduce the concentration of dangling-bond defects which give an electron spin resonance (ESR) signal of $g=2.0055$. However, at least 10^{15}-cm^{-3} defects remain even in device-quality hydrogenated amorphous silicon samples (a-Si:H, 5×10^{22} Si cm^{-3}). Moreover, this material exhibits light-induced metastability (Staebler-Wronski effect).[1] Prolonged light illumination (i.e., light soaking) increases the concentration of the spin active centers by more than one order of magnitude and causes reduction of excess carrier lifetimes. Thermal annealing, typically at 150 °C for 1 h, restores the original low defect concentration. At present, applicability of a-Si:H based solar cells is severely limited by the light-induced degradation which originates from the structural metastability. Elucidation of a microscopic creation mechanism of the photocreated defects is one of the main subjects in a-Si:H both of basic scientific interest and of technological importance.

Typically, 10 at. % bonded hydrogen is contained in a-Si:H film of device quality. It has not been established whether the modification of the amorphous network by the incorporation of hydrogen atoms, which is critically important in lowering the density of dangling-bond defects, causes the metastability or not. In several models proposed in the literature, hydrogen atoms are directly involved in the metastable defect formation in a form such as Si-H bond breaking, local rearrangement of hydrogen configuration, and hydrogen diffusion. To clarify the role of hydrogen in the defect creation, the experimental determination of the spatial relationship between hydrogen atoms and dangling bonds would be crucial. During light illumination of undoped a-Si:H at low temperatures ($\lesssim 150$ K), two light-induced ESR (LESR) signals with g values of 2.004 and 2.013 are observed.[2] The role of these transient states in the metastable defect formation has not been established yet.

In identifying the structure of point defects in semiconductor crystals, ESR is extremely useful by supplying detailed information of the microscopic level. ESR is convenient for determining the concentration of the dangling-bond defects in a-Si:H film. However, in a conventional ESR of the continuous-wave (cw) mode, the spectrum of dangling bonds is inhomogeneously broadened ($\Delta B_{pp}\sim 0.7$ mT at 9.5 GHz), consisting of many overlapping spin packets with different resonant frequencies. Since the linewidth is not affected by deuteration (H: $I=\frac{1}{2}$, $g_n=5.585\,691\,2$; D: $I=1$, $g_n=0.857\,437\,6$), it is inferred that hydrogen is not sited at an immediate neighborhood of the dangling bond such as the backbond position[3,4] (Si-Si=2.35 Å in crystalline silicon). Weak hyperfine interaction, which gives information of the distance between the hydrogen and dangling bond, is completely hidden underneath the inhomogeneous broadening which is caused mainly by distribution of the g value due to both random orientation and site-to-site variation of structure.

In the present work, the weak hydrogen (deuterium) hyperfine interaction has been extracted by using electron-spin-echo envelope modulation (ESEEM) of a pulsed ESR technique which provides a high-frequency resolution because it overcomes inhomogeneous broadening. The ESEEM method has proven to be useful in determining the number and distance of magnetic nuclei within 2–6 Å from the unpaired electron even for a disordered system.[5] We have used deuterated amorphous

silicon (a-Si:D), since D-ESEEM requires less excitation bandwidth of microwave pulses than H-ESEEM. In a randomly oriented system, D-ESEEM persists for a longer time scale than H-ESEEM since hyperfine broadening of the electron nuclear double-resonance (ENDOR) frequency is smaller. D-ESEEM is stronger than H-ESEEM, since the modulation depth is proportional to $I(I+1)$ for small nuclear quadrupole interactions.[5,6] Local arrangement of deuterium (hydrogen) atoms is compared among the native dangling bonds which remain after annealing, the metastable dangling bonds which are created by light soaking, and the transient defects which give LESR signals.

II. WHY ESEEM?

In pulsed ESR, transient signals produced by coherent excitation using microwave pulse(s) are observed in a time domain. The microwave pulse is characterized by the turning angle θ_p through which the microwave field B_1 turns the electron magnetic moment. A strong microwave pulse excites spin packets within $\sim g\beta B_1/h$ of resonance simultaneously, with the microwave frequency set to the center of the spectrum. Signal intensity is measured in the time domain, normally with the magnetic field fixed, as a function of time after the pulse or as a function of the interpulse delay. In a-Si:D, free-induction decay, which corresponds to the Fourier transform (FT) of a cw-ESR spectrum, decays rapidly (lifetime $\sim$20 ns). However, in a two-pulse Hahn echo (90°-τ-180°-τ-echo, τ is scanned), an echo decay which corresponds to FT of a spin packet is observable over a wide 2τ range (Fig. 1). In a three-pulse stimulated echo (90°-τ-90°-T-90°-τ-echo , τ is fixed, T is scanned), an echo decay which is mainly caused by the spin-lattice relaxation persists over a longer time scale. At low temperatures, there is a considerable distribution of spin-lattice relaxation time (T_1). The inversion recovery (180°-t-90°-τ-180°-τ-echo, t is scanned, τ is fixed) curve exhibits a stretched-exponential behavior (Fig. 2).

ESEEM is a periodic variation of the echo intensity

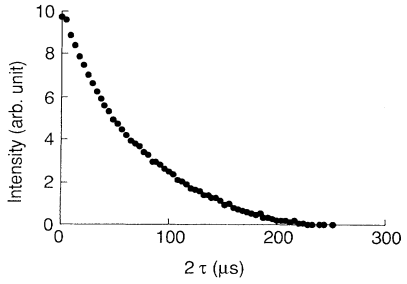

FIG. 1. Phase memory decay curve of the dangling bond ($g=2.0055$) of light-soaked a-Si:D at 56 K. The echo intensity is plotted against time 2τ by using a two-pulse Hahn sequence (90°-τ-180°-τ-echo). This time-domain spectrum corresponds to Fourier transform of a spin packet. Frequency resolution of the spin-packet width is obtainable by using two-pulse electron spin echo.

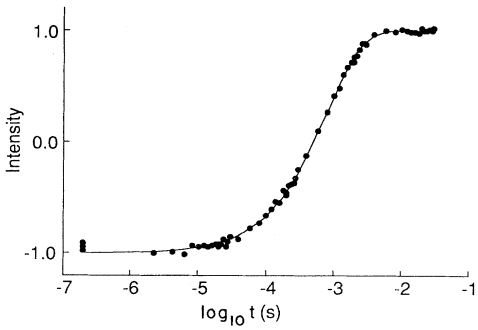

FIG. 2. Inversion recovery curve of the dangling bond ($g=2.0055$) of light-soaked a-Si:D at 56 K. The echo intensity is plotted against time t by using the inversion recovery sequence (180°-t-90°-τ-180°-τ-echo) in which the recovery of M_z (the component of magnetization along the external fixed) is monitored by a two-pulse Hahn echo (τ fixed). The recovery curve is described by a stretched exponential function, $I(t)/I_0=2\exp[-(t/T_1)^{\beta}]-1$ with $T_1=790\ \mu$s, and $\beta=0.83$.

which appears superimposed on the slow echo decays measured by using a pulse sequence of a two-pulse Hahn echo or three-pulse stimulated echo.[5,7-9] If a nuclear spin is sited at a distance which produces dipolar hyperfine interaction comparable to the nuclear Zeeman interaction, a formally forbidden nuclear-spin-flip ($\Delta M_S=\pm1$, $\Delta m_I\neq0$) transition is partially allowed due to state mixing since m_I is not a good quantum number in this case. ESEEM arises from interference effects between allowed and forbidden transitions, both of which are excited by intense microwave pulses. In single-crystal samples, the modulation contains the ENDOR (electron nuclear double-resonance) frequencies ν_α, ν_β and their sum and difference $\nu_\alpha\pm\nu_\beta$ in two-pulse experiments and ν_α, ν_β in three-pulse experiments. The frequency-domain spectrum is obtained by Fourier transform (FT) of the time-domain spectrum after the slow decay due to the spin relaxation is subtracted. In single-crystal samples, since the modulation is observed for many cycles over the wide time range of the echo decay, ENDOR frequencies (i.e., hyperfine interaction and nuclear quadrupole interaction) are measurable to high accuracy.[10] In single-crystal samples, the modulation depth is strongly angular dependent, since the degree of state mixing depends on the angle θ between the external magnetic field and the vector connecting the electron spin and the nuclear spin.[10] The modulation is extremely weak for the principal axis directions ($\theta=0°$, 90°), although echo is observable similarly as at other orientations.

In randomly oriented samples, an ESEEM spectrum is a superposition of spectra at many different orientations, each with different ENDOR frequencies ($\nu_{\mathrm{ENDOR}}=\nu_\alpha,\nu_\beta$) and with different modulation depths. An FT-ESEEM spectrum in the frequency domain usually shows featureless peaks centered at ν_n and at $2\nu_n$ in the two-pulse experiment (Fig. 3) and at ν_n in the three-pulse experiment, where ν_n is the free nuclear precession frequency. Due to the angular dependence of the state mixing, a line shape

from which principal values ($A_{\parallel}, A_{\perp}$) of hyperfine interaction are easily assignable is not obtained. Both the intensity and the linewidth of the ν_n peak strongly depends on the distance r between the electron spin and the nuclear spin. At a relatively small r, although the modulation amplitude at the short time range is large, the modulation in the time domain damps out rapidly reflecting a broad ν_n peak in the frequency domain due to a large distribution of ν_{ENDOR} (Figs. 3 and 4). Thus, the modulation may not be necessarily observed over the whole range of the echo decay. At a relatively large r, although the modulation depth is small since the degree of state mixing is small, the modulation persists over a long time range reflecting a narrow ν_n peak in the frequency domain (Figs. 3 and 4). The line shape of the FT-ESEEM spectrum is often severely distorted due to the dead-time problem of the spectrometer which makes the initial part of the echo decay unobservable. In the randomly oriented sample, determination of both distance and the number of nuclear spins coupled to the electron spin requires simulation of the modulation pattern (the modulation amplitude and its damping behavior) in the time domain.

The modulation pattern of three-pulse ESEEM (Fig. 4) is simpler than that of two-pulse ESEEM, since the $\nu_\alpha \pm \nu_\beta$ components are not involved. Usually, three-pulse ESEEM with slower echo decays supplies higher-frequency resolution than two-pulse ESEEM. Even in randomly oriented samples, the sum frequency ($2\nu_n = \nu_\alpha + \nu_\beta$) peak in two-pulse ESEEM is not broadened, to first order, by distribution of hyperfine interaction [Fig. 3(b)]. The modulation of the $2\nu_n$ component is less hampered by the dead-time problem. The presence of closer nuclei which might be missed by three-pulse ESEEM due to rapid damping of the ν_n component can be checked by the strength of the $2\nu_n$ component in the two-pulse ESEEM.

In obtaining structural information based on ν_{ENDOR}, the ESEEM method is a complement of conventional ENDOR. ESEEM has a limited applicability since there is no modulation effect for a large hyperfine interaction system in which no significant "forbidden" nuclear-spin-flip transitions occur. While signal intensity of conventional ENDOR depends on rather complex relaxation pathways, the intensity of ESEEM is independent of the nuclear and electron spin relaxation rates. In conventional ENDOR of a disordered system, measurement of

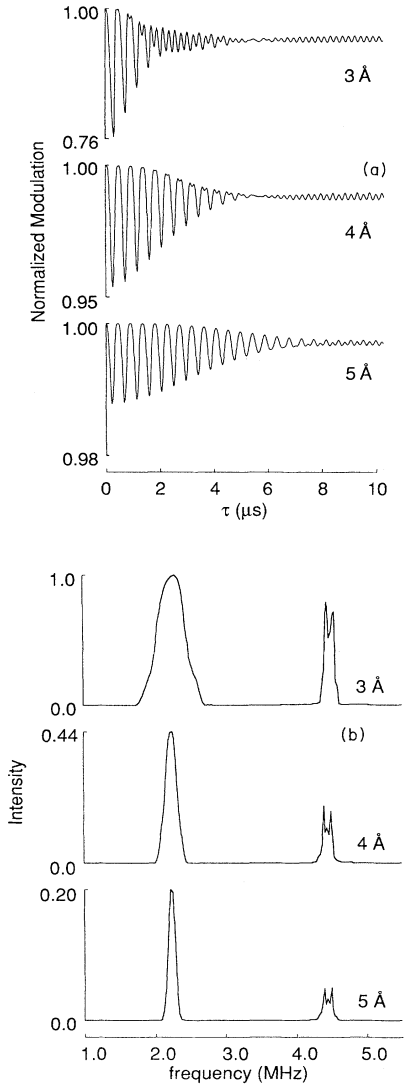

FIG. 3. Calculated two-pulse ESEEM from a single D nucleus ($a_{\mathrm{iso}}=0$, $e^2qQ/h=87$ kHz, asymmetric parameter $\eta=0$) at a distance r from an unpaired electron ($g=2.0055$) in a randomly oriented system (external magnetic field $B=338$ mT). (a) Normalized modulations which are the time-domain spectra without containing echo decay due to spin relaxation; (b) frequency-domain spectra obtained by Fourier transform of time-domain spectra of a wider range (20-ns step, 1024 points).

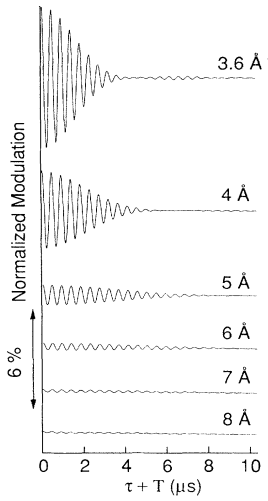

FIG. 4. Calculated normalized modulations of three-pulse ESEEM from a single D nucleus ($a_{\mathrm{iso}}=0$, $e^2qQ/h=87$ kHz, asymmetric parameter $\eta=0$) at a distance r from an unpaired electron ($g=2.0055$) in a randomly oriented system (external magnetic field $B=338$ mT).

the weak hyperfine interaction (matrix-ENDOR) is disturbed by a strong distant-ENDOR signal at ν_n. Hydrogen atoms having isotropic hyperfine interaction $a_{\rm iso}/h=6$ MHz ($a_{\rm iso}/g\beta=0.2$ mT) were detected by using conventional ENDOR in an a-Si:H sample ([H] > 30 at. %, the density of spins: 1.6×10^{18} cm^{-3}) prepared by glow-discharge decomposition of SiH_4 at 70 °C.[11] A model which involves Si·H-Si three-center bonding was presented.[11] So far, except for this high defect density sample, the conventional ENDOR method has failed to detect any hydrogen hyperfine interaction which shifts $\nu_{\rm ENDOR}({\rm H})$ considerably from $\nu_n({\rm H})$.[11–13]

An electron spin experiences a dipolar field from a nearby nuclear spin. The hyperfine interaction due to dipole-dipole interaction (in mT) is

$$A_{\rm dip}/g\beta=g_n\beta_n(3\cos^2\theta-1)/r^3 \ . \tag{1}$$

At $r=3$ Å, $g_n\beta_n/r^3$ is 0.1045 and 0.0160 mT for hydrogen and deuterium, respectively. Thus, if dangling bonds accompany a hydrogen atom(s) at a distance smaller than 3 Å, the cw-ESR linewidth should be affected by deuteration. In films of device quality, since there is essentially no difference in linewidth between a-Si:H and a-Si:D, hydrogen atoms are unlikely to be situated at immediate neighborhood ($r<3$ Å), at least, of the majority of dangling bonds. Thus, hydrogen atoms are located away from the electron spin at a distance which is particularly suited to apply the ESEEM. The modulation depth is sensitive to the distance r, being proportional to r^{-6} for $r>3.6$ Å.[5]

III. EXPERIMENTAL

The powdered sample of a-Si:D (37 mg) was obtained from a thin-film structure which was deposited by the decomposition of SiD_4 gas by a glow-discharge technique on an Al substrate at a temperature of 250 °C. The spin concentration was 3×10^{15} cm^{-3} after annealing and was increased to 1.0×10^{16} cm^{-3} by light soaking. The deuterium concentration measured by NMR was 9.3 at. %.[14]

The pulsed ESR measurements were carried out by using a homebuilt spectrometer equipped with a 1-kW pulsed traveling-wave tube amplifier (TWTA) and a pulse programmer that controlled the interpulse delay(s) with the minimum step of 5 ns and the microwave pulse width(s) with the minimum step of 0.2 ns. The delay between the pulse sequence in data accumulation (repetition delay) can be varied from a minimum 200 μs which is determined by the duty cycle of the limiter and by that of the 1-kW pulsed traveling-wave tube amplifier (TWTA) to a maximum 10 s. Sample temperature was controlled by using an Oxford Instrument ESR-900. ESEEM measurements of LESR signals were carried out by irradiation of a krypton laser ($\lambda=676$ nm) of 4 mW output through a slotted grid of a rectangular TE_{102} mode cavity. Most components in our microwave circuit work in a frequency range of 8.2–12.4 GHz. By switching to one of three Gunn oscillators and by changing the cavity, our pulsed ESR spectrometer can be operated at three different microwave frequencies, 8.5, 9.5, and 11.5 GHz. In a randomly oriented system, geometrical information is extracted from the intensity of ESEEM measured relative to the echo decay curve, rather than the precise measurement of modulation frequency. The base line of the echo decay curve which is critical in measuring weak ESEEM as in the case of a-Si:D was assured by employing phase cycling[15] of microwave pulses. The phase modulation is carried out by a homebuilt 2-bit digital phase shifter which consists of four paths, each equipped with a p-i-n diode switch, attenuator, and phase shifter. The phase settings (normally, 0°, 90°, 180°, 270°) are adjustable by using phase shifters within an accuracy detectable by a Lissajous figure.

ESEEM spectra were recorded at 56 K, which gives a good improvement of the signal-to-noise ratio by accumulation. The sample temperature, which was monitored by a thermocouple in contact with the sample, was stable within 1 K during the measurement. As temperature decreases, the echo intensity increases, while the repetition rate of data accumulation needs to be lowered with the increase of T_1. The repetition rate of the pulse sequence to generate echo was taken to be sufficiently slow (the repetition delay 8 ms), by taking into account the distribution of T_1 (Fig. 2) which might be caused by a slight variation in local surroundings. A repetition rate which is too fast to allow complete relaxation was avoided, since it might selectively collect responses of spins with shorter T_1 by reducing the echo intensity by partial saturation. The microwave pulses used were 50 W in power at 9.5 GHz with 20 and 40 ns wide for 90° and 180° pulses, respectively, which corresponds to the microwave field of $B_1\cong0.45$ mT. The estimation of B_1 as well as the setting of microwave pulse widths was carried out by measuring the echo intensity as a function of the pulse widths.[16] The effective pulse width in the cavity was shorter (by ~25 ns) than the pulse widths applied to p-i-n diode switches. Observation of ESEEM requires $B_1\gtrsim\nu_{\rm ENDOR}$ to excite both "allowed" and "forbidden" transitions. Usually, ESEEM deals with a system with $\nu_{\rm ENDOR}\lesssim1.5g_n\beta_nB/h$. At 350 mT, $g_n\beta_nB/g\beta=0.531$ mT for H and 0.0815 mT for D. Thus, B_1 was sufficiently large to excite D-ESEEM.

IV. RESULTS AND DISCUSSION

A. ESEEM spectra

Nuclear quadrupole interaction of deuterium atoms coupled to electron spin has been determined from two-pulse ESEEM (Fig. 5). The first-order D-ENDOR frequencies are

$$\nu_{\rm ENDOR}(M_S)=\nu_n+M_S\nu_A\pm\nu_Q \ , \tag{2}$$

where ν_A is hyperfine splitting, $2\nu_Q$ is the quadrupole splitting, and M_S is the electron-spin quantum number. The first-order D quadrupole correction, with asymmetric parameter $\eta=0$, to the ENDOR frequency is

$$\nu_Q=\tfrac{3}{8}e^2qQ(3\cos^2\theta_Q-1)/h \ , \tag{3}$$

where θ_Q is the angle between the quadrupole axis and the external magnetic field. The sum frequency

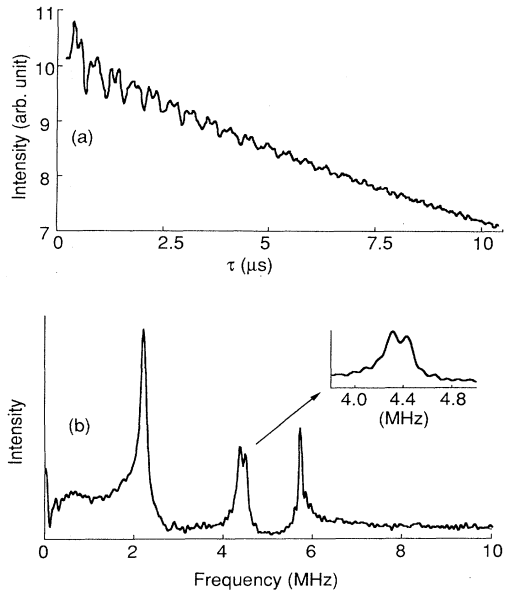

FIG. 5. (a) Two-pulse echo decay and time-domain ESEEM spectrum (9.54 GHz, 56 K) of a photocreated dangling bond ($g=2.0055$) of a-Si:D. (b) FT-ESEEM spectrum showing ν_n(D), $2\nu_n$(D) which has a doublet structure, and $2\nu_n(^{29}\text{Si})$ peaks. The $\nu_n(^{29}\text{Si})$ peak is not observed since the modulation damps out within the dead-time (~ 150 ns) of our pulsed ESR spectrometer.

$2\nu_n \pm 2\nu_Q$, while being free from hyperfine splitting in the weak hyperfine interaction limit, exhibits quadrupole splitting ($4\nu_Q$) twice as large as that ($2\nu_Q$) of the ENDOR frequency. The nuclear quadrupole interaction can be, selectively and with higher resolution, measured from the sum frequency peak. The $2\nu_n$(D) peak in Fig. 5(b) exhibits a line shape typical of the powder spectrum of the axially symmetric quadrupole tensor. The splitting ($\frac{3}{2}e^2qQ/h = 120\pm 10$ kHz) in the $2\nu_n$(D) peak which corresponds to $4\nu_Q$ for the angle between the quadrupole axis and the external magnetic field $\theta_Q = 90°$ is similar for both native and metastable defects.[17] While the NMR method does collect responses of most deuterium atoms in films, information obtained by ESEEM corresponds to NMR of deuterium atoms which are located in the vicinity of the unpaired electron. It should be noted that the quadrupole interaction of deuterium located nearby paramagnetic dangling bonds is similar to that of the majority of deuterium ($e^2qQ/h = 87$ kHz, asymmetric parameter $\eta = 0$) measured by quadrupole echo technique of pulsed NMR for the same a-Si:D sample.[14] The nuclear quadrupole splitting is proportional to the electric-field gradient at the nuclear site. Special deuterium sites which have bonding nature significantly deviated from normal Si-D are unlikely to be involved in the vicinity of the unpaired electron. The same deuterium quadrupole splitting is observed for the LESR defects ($g=2.004$, 2.013).

In three-pulse ESEEM measurements, the modulation from deuterium nuclei is selectively obtained by choosing the value of τ. Since the modulation depth is very small, the time-domain ESEEM spectrum in which the modulation is superimposed on the echo decay [Fig. 5(a) in the case of two-pulse ESEEM] is inconvenient to discuss variation among different dangling-bond defects and to compare with simulated spectra. The ESEEM spectrum is a product of the slow echo decay due to spin relaxation and the normalized modulation which is in a form $1-f(\tau+T)$. The time $(\tau+T)$ dependent part of the normalized modulation is illustrated in Fig. 6. The normalized modulation observed is similar for the native dangling bond and the metastable dangling bonds. The deuterium hyperfine interaction which causes ESEEM depends not only on local arrangement of deuterium but also on the extent of the wave function of the unpaired electron. Dangling-bond defects are considered to involve a threefold-coordinated silicon. Since the ^{29}Si hyperfine splitting which is assigned to the threefold-coordinated silicon is observed to be similar,[18] the local arrangement of deuterium atoms in the vicinity of the native and the metastable dangling bonds is similar.

The modulation depth of LESR is considerably weaker than that of dangling bonds (Fig. 6). The modulation pattern is similar between two kinds of LESR signals ($g=2.004$ and 2.013). The echo-detected ESR in which the echo intensity was measured as a function of the magnetic field revealed that the LESR signals have ^{29}Si hyperfine splitting similar to that of the dangling bond.[19] Thus, it is likely that the LESR signals originate from localized states similar to the dangling-bond defects. If the extent of the wave function of the unpaired electron is the same between dangling-bond defects and the LESR

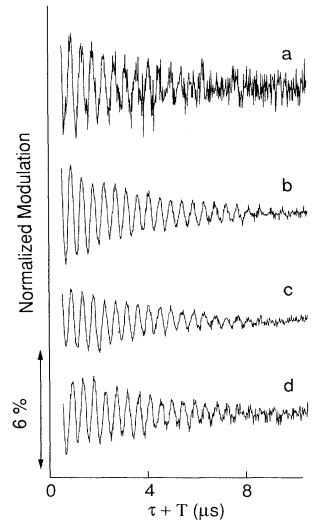

FIG. 6. Three-pulse ESEEM spectra ($\tau=220$ ns, 9.54 GHz, 56 K) of a-Si:D. The $(\tau+T)$-dependent component of the normalized modulation is shown. The modulation amplitude is expressed as a fraction relative to the echo intensity. (a) Dangling bond ($g=2.0055$) after annealing (accumulation of 3×10^4 sweeps, each consists of 512 pionts of $\tau+T$). (b) Dangling bond ($g=2.0055$) after light soaking (accumulation of 1×10^4 sweeps). (c) LESR ($g=2.004$) after annealing. (d) LESR ($g=2.013$) after annealing.

states, the local concentration of deuterium is lower in LESR states than in the dangling-bond defects.

B. Simulation of ESEEM

The distance between the dangling bond and deuterium was estimated by computer simulation of the modulation pattern. ESEEM is directly related to the spin Hamiltonian.[20] If the spin Hamiltonian is constructed from a given geometrical model, ESEEM can be calculated in a straightforward manner. Since ESEEM is caused by weak hyperfine interaction, we encounter a situation in which hyperfine interaction might be comparable in magnitude to nuclear Zeeman interaction and/or nuclear quadrupole interaction. ESEEM from a $S=\frac{1}{2}$, $I=1$ system is, often, analyzed by neglecting the quadrupole interaction,[5] by using an approximate formula,[6] or by using the perturbation method.[21] Here, the normalized modulation is calculated from eigenvalues and eigenvectors which are obtained by diagonalization of the spin-Hamiltonian matrix. The normalized modulation of two-pulse ESEEM ($S=\frac{1}{2}$) is[20,22]

$$E(\tau)=\frac{1}{2I+1}\left[\sum_{i,k}|M_{ik}|^4+2\sum_{(i<j),k}|M_{ik}|^2|M_{jk}|^2\cos\omega_{ij}\tau+2\sum_{i,(k<n)}|M_{in}|^2|M_{ik}|^2\cos\omega_{kn}\tau\right.$$
$$+2\sum_{(i<j),(k<n)}\mathrm{Re}(M_{jk}^*M_{jn}M_{in}^*M_{ik})\cos(\omega_{ij}+\omega_{kn})\tau$$
$$\left.+2\sum_{(i<j),(k<n)}\mathrm{Re}(M_{ik}^*M_{in}M_{jn}^*M_{jk})\cos(\omega_{ij}-\omega_{kn})\tau\right]. \tag{4}$$

The normalized modulation of three-pulse ESEEM ($S=\frac{1}{2}$) is[20,22]

$$E(\tau,T)=\frac{1}{2I+1}\left\{\sum_{i,k}|M_{ik}|^4+\sum_{i<j}\left[\sum_k|M_{ik}|^2|M_{jk}|^2\right][\cos\omega_{ij}\tau+\cos\omega_{ij}(\tau+T)]\right.$$
$$+\sum_{k<n}\left[\sum_i|M_{ik}|^2|M_{in}|^2\right][\cos\omega_{kn}\tau+\cos\omega_{kn}(\tau+T)]$$
$$\left.+2\sum_{i<j}\sum_{k<n}(\mathrm{Re}[M_{ik}^*M_{in}M_{jn}^*M_{jk}])[\cos\omega_{ij}(\tau+T)\cos\omega_{kn}\tau+\cos\omega_{ij}\tau\cos\omega_{kn}(\tau+T)]\right\}. \tag{5}$$

The matrix element M_{ik} maps the nuclear eigenvector of the $M_S=+\frac{1}{2}$ manifold into the nuclear eigenvector of the $M_S=-\frac{1}{2}$ manifold. The ENDOR frequencies (in angular frequency $\omega=2\pi\nu$) $\omega_{ij}=\omega_i-\omega_j$ and $\omega_{kn}=\omega_k-\omega_n$ are those of the $M_S=+\frac{1}{2}$ manifold and those of the $M_S=-\frac{1}{2}$ manifold, respectively. The eigenvector of the ith eigenstate ($M_S=+\frac{1}{2}$) is expressed as

$$\psi_i=f_{i,1}|+\tfrac{1}{2},1\rangle+f_{i,0}|+\tfrac{1}{2},0\rangle+f_{i,-1}|+\tfrac{1}{2},-1\rangle\ . \tag{6}$$

Using the vector $\mathbf{F}_i$ which has the components of complex numbers $f_{i,1}$, $f_{i,0}$, and $f_{i,-1}$, M_{ik} is given by[19]

$$M_{ik}=\mathbf{F}_i^\dagger\cdot\mathbf{F}_k\ . \tag{7}$$

The normalized modulation from an orientation $(\theta,\phi,\theta_Q,\phi_Q)$ of a deuterium nucleus at a distance r is calculated from the eigenvalues and eigenvectors which are obtained by diagonalization of a 6×6 complex Hermitian matrix of the spin Hamiltonian ($S=\frac{1}{2}$, $I=1$)

$$\mathcal{H}=g\beta_e\mathbf{S}\cdot\mathbf{B}+g_n\beta_n\mathbf{I}\cdot\mathbf{B}+\mathbf{S}\cdot\mathbf{A}\cdot\mathbf{I}+\mathbf{I}\cdot\mathbf{Q}\cdot\mathbf{I}\ , \tag{8}$$

where (θ,ϕ) and (θ_Q,ϕ_Q) are the direction of the hyperfine axis and that of the nuclear quadrupole axis, respectively. In our case, off-diagonal elements in the electron spin can be neglected, since the electron Zeeman interaction is much larger than any other terms in the spin Hamiltonian. In this high-field approximation, calculation is reduced to diagonalization of two 3×3 submatrices. We assumed isotropic g, thus the electron spin is taken to be quantized along the external magnetic field. In constructing the spin-Hamiltonian matrix to be diagonalized, we use a xyz Cartesian coordinate system which is the principal axis system of the hyperfine tensor $\mathbf{A}$. The spin Hamiltonian is

$$\mathcal{H}(M_S)=g\beta BM_S+\sin\theta_B\cos\phi_B[g_n\beta_nB+M_SA_x]I_x+\sin\theta_B\sin\phi_B[g_n\beta_nB+M_SA_y]I_y$$
$$+\cos\theta_B[g_n\beta_nB+M_SA_z]I_z+\tfrac{1}{2}(Q_{xx}-Q_{yy})(I_x^2-I_y^2)+\tfrac{1}{2}Q_{zz}[3I_z^2-I(I+1)]$$
$$+Q_{xy}(I_xI_y+I_yI_x)+Q_{yz}(I_yI_z+I_zI_y)+Q_{zx}(I_zI_x+I_xI_z)\ , \tag{9}$$

where (θ_B,ϕ_B) is the direction of the external magnetic field. The principal values A_x, A_y, A_z ($A_x = A_y$ in our case) of the hyperfine tensor were calculated by point-dipole approximation [Eq. (1)]. The small isotropic part ($a_{\rm iso}$) was included when it was necessary to include a small overlap of the unpaired electron wave function at the deuterium nucleus. The nuclear quadrupole tensor is taken to be axially symmetric ($\eta=0$) around direction (θ_D,ϕ_D) which, presumably, coincides with the Si-D direction. The principal values of the nuclear quadrupole tensor were taken to be the same as those obtained by NMR. The hyperfine tensor and the nuclear quadrupole tensor are not colinear. The elements of the quadrupole tensor in the *xyz* system are obtained by similarity transformation.

The simulation $E(r,a_{\rm iso})$ for random orientations of a single deuterium $(r,a_{\rm iso})$ is obtained as superpositions of many orientations.[5] Since the hyperfine tensor is axially symmetric, in our case, the orientations were taken from a grid of θ_B-θ_D-ϕ_D space. The overall modulation for the case that many deuterium nuclei $(n_i,r_i,a_{{\rm iso}_i})$ $(i=1,2,\ldots,n)$ are coupled to the same electron spin was obtained as the product of the individual modulation functions,[5]

$$E=(E_1(r_1,a_{{\rm iso}_1}))^{n_1} \times(E_2(r_2,a_{{\rm iso}_2}))^{n_2}\cdots(E_n(r_n,a_{{\rm iso}_n}))^{n_n}, \qquad (10)$$

where n_i denotes n_i equivalent nuclei at distance r_i. An approximation that the relative positions of nuclei are uncorrelated was used. In the calculated spectra to be described below, spectra at 65 650 orientations were added to obtain each E_i $(r_i, a_{{\rm iso}_i})$.

First, we describe the simulation for the dangling bonds with $g=2.0055$. The features of the three-pulse normalized modulation pattern is characterized by both the modulation amplitude in the small $\tau+T$ range and the damping behavior of the modulation. In the simulated spectrum with a single deuterium nucleus at $r=3.9$ Å, the modulation amplitude at the small $\tau+T$ range is similar to that of the observed spectrum, while the modulation damps faster than that of the observed spectrum. A good fitting to the observed modulation pattern was not obtained with a single D nucleus. The simulation of the normalized modulation arising from n equivalent D nuclei at a distance r was calculated for many sets of (n,r). The modulation amplitude at the small $\tau+T$ range is reproduced by several sets of (n,r) [(2, 4.4 Å), (4, 5 Å), (12, 6 Å)]. Comparing with the observed pattern, the simulated modulation pattern with small r damps too fast and the simulated pattern with large r damps too slow. Thus, in order to get a better fit to the experimental observation, we need distant deuterium in addition to closely located deuterium. As shown in Fig. 7, a good fitting was obtained by one D nucleus at 4.2 Å ($a_{\rm iso}=0.05$ MHz) or two D nuclei at 4.8 Å ($a_{\rm iso}=0.05$ MHz) in addition to a set of distant nuclei ($a_{\rm iso}=0$, 6 Å, $n=1$, 7 Å, $n=2$, 8 Å, $n=8$). Six deuterium nuclei (6 Å, $n=1$, 7 Å, $n=2$, 8 Å, $n=3$) represent ~6 at. % occupancy by deuterium nuclei of silicon sites from $r=5$ Å to $r=8$ Å. Five deuterium nuclei (8 Å, $n=5$) are added to include deuterium nuclei at $r>8$ Å. The isotropic part $a_{\rm iso}=0.05$ MHz corresponds to a fraction 2.3×10^{-4} of the 1*s* orbital. A good fitting was not obtained by more than three closest D nuclei.

In a randomly oriented system, a broadening of modulation frequency which is caused by a distribution of $\nu_{\rm ENDOR}$ causes the modulation to damp out. In the FT-ESEEM spectrum shown in Fig. 5(b), $\nu_n(^{29}{\rm Si})$ is not observed, while the $2\nu_n(^{29}{\rm Si})$ peak is clearly seen. The modulation component of $\nu_n(^{29}{\rm Si})$ damps rapidly within the dead-time (~150 ns) of our spectrometer due to relatively strong hyperfine interaction. Modulation which has a width $\Delta\nu=1/(2\pi\times150\ {\rm ns})=1.06$ MHz in the frequency domain is significantly lost within the dead-time (~150 ns). The dead-time does not affect severely deuterium atoms at $r>3$ Å ($g\beta g_n\beta_n/hr^3=0.45$ MHz at $r=3$ Å). As seen from Fig. 3(a), even if the initial part of $\tau\lesssim0.5$ μs were missing in a two-pulse ESEEM, it is expected that the modulation from deuterium at $r=3$ Å should overwhelm that from deuterium at $r>4$ Å in the range of $0.5\mu{\rm s}<\tau<1.5$ μs. Furthermore, the possibility of missing a presence of closer deuterium atoms can be checked from the intensity of $2\nu_n$(D) modulation in two-pulse ESEEM, since the $2\nu_n$(D) peak is not broadened, to first order, by distribution of $\nu_{\rm ENDOR}$. In two-pulse ESEEM, the value of τ from which $2\nu_n$(D) modulation dominates over ν_n(D) modulation decreases as r de-

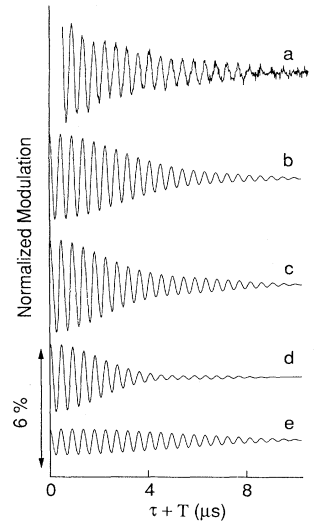

FIG. 7. Simulated three-pulse normalized modulation ($e^2qQ/h=87$ kHz, asymmetric parameter $\eta=0$ for all D nuclei). (a) Observed normalized modulation of the photocreated dangling bond ($g=2.0055$). (b) Calculated normalized modulation with one D nucleus at 4.2 Å ($a_{\rm iso}=0.05$ MHz) in addition to a set of distant *D* nuclei. (c) Calculated normalized modulation with two D nuclei at 4.8 Å ($a_{\rm iso}=0.05$ MHz) in addition to a set of distant D nuclei. (d) Calculated normalized modulation with one D nucleus at 4.2 Å ($a_{\rm iso}=0.05$ MHz). (e) Calculated normalized modulation from a set of distant D nuclei ($a_{\rm iso}=0$, 6 Å, $n=1$, 7 Å, $n=2$, 8 Å, $n=8$).

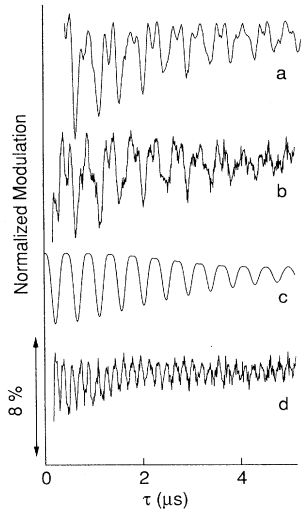

FIG. 8. Two-pulse normalized modulation of (a) the observed spectrum for the dangling bond ($g=2.0055$) of a-Si:D after light soaking. (b) Product of (c) and (d). (c) Simulated spectrum with one D nucleus at 4.2 Å ($a_{iso}=0.05$ MHz) in addition to a set of distant D nuclei ($a_{iso}=0$, 6, Å, $n=1$, 7 Å, $n=2$, 8 Å, $n=8$). ($e^2qQ/h=87$ kHz, asymmetric parameter $\eta=0$ for all D nuclei.) (d) Observed spectrum for the dangling bond ($g=2.0055$) of a-Si:H after light soaking.

creases [Fig. 3(a)]. At first sight, the two-pulse ESEEM observed might seem to have a $2\nu_n$(D) component which appears distinctly from a small τ value [Figs. 5(a) and 8(a)]. However, the high-frequency component which appears distinctly from a small τ value is not $2\nu_n$(D) modulation but $2\nu_n(^{29}\text{Si})$ modulation. The two-pulse normalized modulation due to ^{29}Si was obtained experimentally from two-pulse ESEEM of a-Si:H, in which H-ESEEM could be effectively suppressed by using relatively low microwave pulse power [Fig. 8(d)]. A simulated two-pulse modulation pattern was obtained as the product of the normalized modulation of a-Si:H obtained experimentally and the normalized modulation calculated for the set of D nuclei. A good fitting of the two-pulse ESEEM spectrum was attained by using the same set of the D nuclei arrangement which was determined from the three-pulse ESEEM simulation (Fig. 8). Thus, the presence of close deuterium nuclei of which modulation at frequency ν_n damps out in the dead time is unlikely, at least, for the majority ($\gtrsim 90\%$) of the dangling bonds in the device-quality sample used.

For the modulation observed for the LESR signal of $g=2.004$, a good agreement between simulation and the observed spectrum was obtained by setting either one D nucleus at 4.8 Å ($a_{iso}=0.05$ MHz) or two D nuclei at 5.3 Å ($a_{iso}=0$), using the same set of distant deuterium nuclei as that used for simulation of the dangling bond with $g=2.0055$. Between two LESR signals ($g=2.004$ and 2.013), the distance to the closest deuterium nucleus is similar since the modulation pattern is similar.

C. Local hydrogen arrangement

In the random network of amorphous material, it is expected that the arrangement of deuterium in the vicinity of the unpaired electron should have a considerable site-to-site variation. In our simulation, an average arrangement is represented by a set of D nuclei in which D nuclei are placed at discrete distances. Since the modulation depth increases drastically as the distance decreases [Figs. 3(a) and 4], it is likely that the distance of 4.2 Å of the closest deuterium (4.8 Å in the case of two closest deuterium nuclei) determined by simulation should be valid for the majority of the dangling bonds ($g=2.0055$) in the device-quality sample used.

In our previous work,[17] the distance to deterium was estimated from simulation of the frequency-domain spectrum (FT-ESEEM spectrum) of two-pulse ESEEM. The frequency-domain spectrum for a orientation (θ_B,θ_D,ϕ_D) of a single deuterium nucleus(r,a_{iso}) was obtained as peaks of a Lorentzian line shape (the linewidth taken from the slow decay due to relaxation) at the modulation frequencies (ENDOR frequencies and their sum and difference frequencies) with the intensities corresponding to the modulation amplitudes. The frequency-domain spectrum for random orientations of a single deuterium nucleus (r,a_{iso}) was obtained as superpositions of many orientations. The distance was estimated from the linewidth of the ν_n(D) peak. Since we overlooked, partly due to the distortion of the FT-ESEEM spectrum caused by missing the initial part of the echo decay due to the dead-time, the contribution from the closest D nuclei which constitutes a broad base of the ν_n(D) peak, a somewhat larger distance (~ 5 Å) was obtained. In the present work, the distance has been estimated by simulation of the time-domain spectra of three-pulse ESEEM.

The distance estimated by ESEEM using a-Si:D is generalized to a-Si:H, which should be justified because of the similarity of the chemical nature between H and D. In crystalline silicon, each silicon is surrounded by 4 nearest neighbors at 2.35 Å, by 12 second nearest neighbors at 3.84 Å, and by 12 third nearest neighbors at 4.50 Å. We note no hydrogen within the distance (3.84 Å) of the second nearest silicon and at most one hydrogen within the distance of 4.2 Å (28 silicon neighbors within 4.5 Å in crystalline silicon). By considering the deuterium content (9.3 at. %), it is inferred that paramagnetic dangling-bond defects are formed in the hydrogen-depleted region of the amorphous network, for both native and photo-created defects.

The distance r used in the simulation of ESEEM spectra is the distance between the unpaired electron and deuterium nuclei by using the point-dipole approximation. This distance equals the distance beetween the threefold-coordinated silicon and hydrogen nuclei in the case of 100% spin localization. Here, possible hydrogen sites are discussed, including delocalization of the unpaired electron. From the analysis of ^{29}Si hyperfine splitting, the fraction of the wave function of the unpaired electron on the dangling-bond silicon is estimated to be 0.5–0.8.[3,23,24] Here, possible hydrogen sites near the dangling bond are discussed, by assuming 70% spin density on the dangling-bond silicon and 10% spin density on each of the three backbond silicon atoms. Effective distance r_{eff} is obtained so that the largest principal value of hyperfine tensor at a distance r_{eff} with 100% localization should be

equal to that of the sum of four hyperfine tensors, each calculated from dipolar interaction (point-dipole approximation) between hydrogen and spin density on each of the four silicon atoms. When the delocalization of the unpaired electron is taken into account, r_{eff} is compared with the distance obtained by simulation. We use the atomic arrangement of the lattice of crystalline silicon. Hydrogen is placed with the Si-H bond (length 1.48 Å) parallel to the corresponding Si-Si direction. From relatively large p character ($p/s \sim 9$),[3,23] it is likely that a structural relaxation with the dangling-bond silicon moved into the plane of backbond silicons is involved. Calculation of r_{eff} was carried out for both unrelaxed and relaxed positions of the dangling-bond silicon.

On the backbond side, the hydrogen bonded to backbond silicon, which is closer than the second nearest silicon (3.84 Å), is excluded. We consider hydrogen sites (labeled $B1$, $B2$, $B3$, $B4$, $B5$, respectively, with two equivalent $B1$ sites as illustrated in Fig. 9) in which the hydrogen atom is bonded to the second nearest silicon atom. The distance between the hydrogen atom and the dangling-bond silicon is $B1$(4.12 Å), $B2$(5.12 Å), $B3$(5.12 Å), $B4$(4.12 Å), and $B5$(4.12 Å). If the dangling-bond silicon is moved into the plane of three back-bond silicon atoms, the distance becomes $B1$(3.44 Å), $B2$(4.60 Å), $B3$(5.11 Å), $B4$(4.10 Å), $B5$(4.46 Å). The effective distance r_{eff} is $B1$(4.24 Å), $B2$(4.86 Å), $B3$(4.87 Å), $B4$(4.25 Å), and $B5$(4.27 Å) for the unrelaxed dangling-bond silicon position, and $B1$(3.68 Å), $B2$(4.57 Å), $B3$(4.84 Å), $B4$(4.21 Å), and $B5$(4.48 Å) for the relaxed position. Thus, at the backbond side, the closest hydrogen site is the one bonded to the second nearest silicon atom.

Now, we consider [Si_3-Si(1)·Si(2)-H] in which the hydrogen atom is bonded to close silicon on the side opposite to that of the backbond silicon atoms. Three-center bonding [Si·H-Si] in which the hydrogen atom is situated between two silicon atoms is excluded, since the distance is too close. Thus, the hydrogen atom needs to be bonded to Si(2) from the side opposite to Si(1). It is assumed that the wave function of the unpaired electron should not be delocalized onto Si(2). In the site labeled $F1$, Si(1)·—Si(2)-H is linear, by assuming that Si(1)-Si(2) bond breaking occurs by attachment of the hydrogen atom to Si(2) from the rear side (Fig. 9). At the site labeled $F2$, Si(2)-Si, which is the "backbond" of Si(2), is replaced with Si(2)-H (Fig. 9). The distance between the hydrogen atom and dangling-bond silicon Si(1) is $F1$(3.83 Å) and $F2$(3.17 Å) for the unrelaxed Si(1) position and $F1$(4.61 Å) and $F2$(3.89 Å) for the relaxed Si(1) position. If delocalization of the unpaired electron preferentially onto the backbond side [i.e., onto Si_3-Si(1)] as well as the dangling-bond silicon Si(1) relaxation into the backbond-silicon plane is included, these sites are acceptable with the distances r_{eff} $F1$(4.86 Å) and $F2$(4.13 Å). If structural relaxation such as inversion of the Si(2)-Si_3 pyramid that moves Si(2) away from Si(1) occurs, r_{eff} is $F1$(5.73 Å) and $F1$(6.39 Å) for unrelaxed and relaxed Si(1) positions, respectively. Thus, a configuration of [Si(1)·Si(2)-H] is acceptable if Si(2)-H points to a direction opposite to the Si(1) side and if the wave function of the unpaired electron is confined to Si(1) and its backbond side.

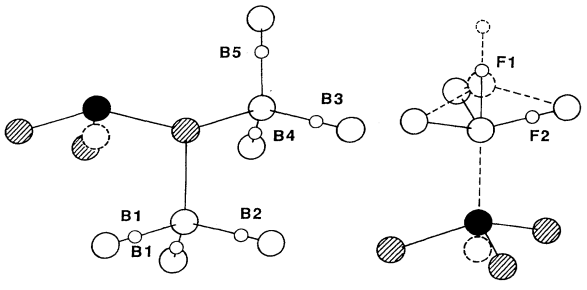

FIG. 9. Possible hydrogen sites near the dangling-bond silicon. Dangling-bond silicon, backbond silicon, and the hydrogen site are illustrated by the solid circle, shaded circle, and small circle, respectively. When Si-H (bond length 1.48 Å) replaces Si-Si, the corresponding Si is removed.

We note that deuterium atoms in the vicinity of the unpaired electron exhibit nuclear quadrupole splitting similar to that of bulk Si-D measured by NMR. Three-center bonding [Si·H-Si] in which the hydrogen atom is sited between two close silicon atoms, is, again, excluded, since the electric-field gradient at the hydrogen nucleus in such a configuration should be significantly deviated from normal Si-D. In addition to the three-center bonding [Si·H-Si] in which both an unpaired electron and hydrogen atom are involved, diamagnetic three-center bonding $[\text{Si-H-Si}]^+$ is unlikely at least near the unpaired electron.

D. Microscopic mechanism of the Staebler-Wronski effect

A photoinduced increase in the density of ESR-active ($g = 2.0055$) defects (Staebler-Wronski effect) is associated with a decrease in photoconductivity and dark conductivity due to a Fermi-level movement to midgap, with an increase in defect photoluminescence and in the density of midgap states. The metastable defects are created by illumination with a threshold energy near $h\nu \geq 1.2$ eV.[25] Activation energy of annealing is determined from temperature dependence of the decay of the photocreated defects. Stutzmann, Jackson, and Tsai reported that the decay is monomolecular with a broad distribution (0.9–1.3 eV) of activation energies.[25] Lee, Ohlsen, and Taylor concluded that the decay is bimolecular with an activation energy of ~ 1 eV.[26] Several different mechanisms have been proposed to explain photoinduced metastability. Our observations will serve both to examine and to refine these defect creation models.

By prolonged exposure to band-gap light, the paramagnetic dangling bonds which are attributed to neutral threefold-coordinated silicon atoms (D^0) are created from diamagnetic precursors without evolving hydrogen out of films. Either bond breaking or change of the charge state (electron or hole trapping) is required to create unpaired electrons. The models proposed are divided into two groups, one which involves a bond breaking to create a pair of paramagnetic dangling bonds and

the other which assumes that paramagnetic dangling bonds are created at locations sufficiently separated from each other.

If dangling bonds are created in a pair which is separated by R, the dipole-dipole interaction between electron spins (in mT)

$$A_{\rm dip}/g\beta = g\beta(3\cos^2\theta - 1)/R^3 \quad (11)$$

causes broadening of the cw-ESR spectrum, where θ is the angle between the external magnetic field and the vector connecting the two spins. At $R = 10$ Å, $g\beta/R^3$ is 1.86 mT. Dersch, Stake, and Beichler concluded that the distance between the photocreated spins is relatively large, at least 10 Å by using the cw-ESR linewidth as an upper limit of dipolar broadening.[27] The long phase-memory time ($T_M \sim 75$ μs; see Fig. 1) with the absence of instantaneous spectral diffusion[28,29] suggests that contribution to inhomogeneous broadening from dipolar interaction among electron spins is negligibly small in the device-quality sample used. In both native and photocreated defects, the electron spins are separated from one another by a distance far more than the minimum distance (10 Å) estimated from the cw-ESR linewidth. Simple breaking of the weak Si-Si bond creates two dangling bonds closely situated to each other, which seems unlikely to be stable. Thus, local rearrangement of the hydrogen configuration is incorporated into weak Si-Si bond breaking by nonradiative recombination of photoexcited carriers.[25,30] These models assume that one of two dangling bonds is terminated by a hydrogen atom which is switched over from an adjacent Si-H bond, leaving two dangling bonds with a somewhat larger distance. It seems that the local rearrangement of hydrogen configuration needs to be followed by a continuous exchange of a hydrogen atom to attain a sufficient distance between dangling bonds. The macroscopic diffusion of hydrogen in a-Si:H is activated with an energy of 1.2–1.5 eV,[31,32] while temperature dependence of the growth curve of photocreated defects indicates that the growth is nearly temperature independent.[25] It has not yet been clarified whether hydrogen migration which causes a relatively large spatial separation between two dangling bonds is feasible or not. Dissociation of the diatomic hydrogen complex [Si_3Si-H H-$SiSi_3$] to form a pair of Si·H-Si dangling bonds,[33] one by dissociation of Si-H and the other by trapping of dissociated hydrogen at a strained Si-Si bond, also requires one to prove that high mobility of the hydrogen atom to separate two dangling bonds sufficiently is feasible. The mechanism of generation of a pair of dangling bonds and floating bonds overcomes the problem of attaining a sufficient separation of electron spins through high mobility of the floating bonds proposed.[34] However, it seems that at present the existence of floating bonds in a-Si:H is still controversial.

As far as the distance between electron spins is concerned, the models that the paramagnetic dangling-bond defects (D^0) are created at existing charged diamagnetic dangling-bond sites (D^+,D^-) that originate from negative effective electronic correlation energy $U_{\rm eff}$ (Ref. 35) or from potential fluctuation[36] seem more probable. In these models, without the necessity of including diffusion, the photocreated paramagnetic dangling bonds are likely to be spatially separated from one another, provided that the charged dangling bonds as precursors are spatially separated. It was suggested that Si-H-Si three-center bonding should have negative-$U_{\rm eff}$ properties in a-Si:H.[37] Except for the case of three-center bonding, a microscopic structural picture which includes the role of hydrogen atoms has not been given yet. Since the present ESEEM results suggest that the dangling-bond defects are created in the hydrogen-depleted region, it seems that the charged dangling bonds which are precursors of photocreated paramagnetic dangling bonds are required to be formed in the hydrogen-depleted region.

Several mechanisms proposed involve Si(1)·H-Si(2), to be denoted here as [Si(1)-H-Si(2)]^0, in which the dangling bond and Si-H are, more or less, facing each other. In the model of weak Si-Si bond breaking associated with local rearrangement of hydrogen, two types of dangling bonds, Si· and [Si(1)-H-Si(2)]^0, are created.[25,30] By a scheme in which a hydrogen atom is released from Si-H, diffuses some distance, and breaks a weak Si-Si bond, two types of dangling bonds, Si· and [Si(1)-H-Si(2)]^0, are created.[38] In the model of dissociation of [Si_3Si-H H-$SiSi_3$], a pair of [Si(1)-H-Si(2)]^0 is created.[33] Capture of an electron by diamagnetic [Si(1)-H-Si(2)]$^+$ or capture of a hole by diamagnetic [Si(1)-H-Si(2)]$^-$ creates [Si(1)-H-Si(2)]^0.[39,40] The ESR spectrum of a neutral interstitial hydrogen atom (H_i^0) at the bond-centered position in crystalline silicon has been reported (H hyperfine interaction $a_{\rm iso}/h = \pm 23.0$ MHz, $b/h = \mp 8.4$ MHz).[41] With a bond-centered configuration of [Si(1)-H-Si(2)]^0, the unpaired electron delocalizes onto two silicon atoms with a fraction of 0.21 of the wave function on each of the two silicon atoms. A simple molecular orbital of a three-center bond Si-H-Si is constructed from a H 1s orbital and two hybrid orbitals of Si atoms. Among the three electrons in the neutral paramagnetic [Si(1)-H-Si(2)]^0, two electrons occupy a bonding state. The unpaired electron occupies a nonbonding state, having a node between the Si atoms, which does not couple to the H 1s orbital.[37] In [Si(1)-H-Si(2)]^0 of crystalline silicon, the Si-Si bond expands by about 34% to accommodate an interstitial hydrogen.[42] In the [Si(1)-H-Si(2)]^0 model of the dangling bond, a large structural relaxation which confines the unpaired electron on the Si(1) side needs to be incorporated to attain both sufficiently large $r_{\rm eff}$ and a bonding character of Si(2)-H similar to that of normal Si-H. We denote, here, the threefold-coordinated silicon on which the unpaired electron is predominantly localized as Si(1). In x-ray-irradiated α-quartz (SiO_2), two types of [O_3Si-H-SiO_3]^0 centers, labeled E_4' and E_2' are produced, presumably by H-atom diffusion to the oxygen vacancy [O_3Si:SiO_3]^0.[43,44] In the oxygen vacancy of the unrelaxed configuration, the Si-Si distance is 3.06 Å with the Si-(oxygen-vacancy)-Si angle of 143.6°. E_4', which has a hydrogen atom between two silicon atoms, exhibits a relatively large H hyperfine interaction ($a_{\rm iso}/h = 18.2$ MHz, $b/h = 17.6$ MHz at room temperature). Small H hyperfine interaction ($a_{\rm iso}/h = 1.2$ MHz, $b/h = 1.7$ MHz at room temperature) in E_2' is attributed to a structural relaxation which causes an inversion of the H-SiO_3 py-

ramid.[44] Thus, E_2' should be denoted as $[O_3Si\cdot/O_3Si\text{-}H]^0$. While an unpaired electron is shared by two silicon atoms in E_4', it is localized predominantly on a silicon atom in E_2'. The $[Si(1)\text{-}H\text{-}Si(2)]^0$ configuration of E_4' which has a hydrogen atom situated between two silicons is considered as an example of hydrogen bonding. The temperature dependence of the H- and ^{29}Si-hyperfine interaction of E_4' in α-quartz is ascribed to hydrogen motion in a double-minimum potential of hydrogen bonding $[Si(1)\text{-}H\text{-}Si(2)]^0$.[43] If a large Si-Si distance is achieved, two electrons occupy the Si(2)-H bonding orbital and the wave function of the unpaired electron contains no admixture of Si(2).[43] If the dangling bond in a-Si:H is originated from an $[Si(1)\text{-}H\text{-}Si(2)]^0$ configuration, the dangling bond Si(1)$\cdot$must be effectively separated from Si(2)-H. It is estimated that $[Si(1)\text{-}H\text{-}Si(2)]^0$ can be treated as two entities, a dangling bond and Si-H, for a Si-Si distance larger than 3.8 Å even if the hydrogen atom is located between two silicon atoms.[39] However, if the hydrogen atom is located between two silicon atoms, unreasonably large elongation of the Si-Si distance is required to attain a large distance to the hydrogen atom ($r_{\text{eff}}=4.2$ Å). The large distance to the hydrogen atom is attainable without requiring an extremely long Si-Si distance if Si(2)-H points to a direction opposite to the Si(1)$\cdot$ side. It is likely that the models which involve dangling bonds of an $[Si(1)\text{-}H\text{-}Si(2)]^0$ configuration need to include a large structural relaxation such as inversion of the $H\text{-}Si(2)Si_3$ pyramid. Thus, although the dangling-bond defects have the same charge state as $[Si(1)\text{-}H\text{-}Si(2)]^0$, the hydrogen atom is not likely to be located between two silicon atoms. In crystalline silicon, it is predicted that an isolated interstitial hydrogen has two configurations, a bond-centered position which is the stable one for H_i^+ and H_i^0 and a tetrahedral interstitial site which is the stable one for H_i^-.[45] In the amorphous network of a-Si:H, the dangling-bond defects might correspond to H_i^0 of another configuration in which Si-H accompanies Si$\cdot$ at a relatively separated position.

The role of transient states which give LESR signals in the formation of metastable dangling bonds has not been clarified yet. No experimental confirmation that a small fraction of LESR states might be converted to metastable dangling bonds, presumably, by attaining further structural relaxation has been reported. We note that the distance to the closest hydrogen atom in the LESR states is larger than that in the metastable dangling bonds. If the metastable dangling bonds are originated from the LESR states, it seems that a structural relaxation which moves the hydrogen atom somewhat closer to the unpaired electron is involved. Since the LESR signals exhibit ^{29}Si hyperfine splitting similar to that of the dangling-bond defects ($g=2.0055$), it is likely that a significant part of the wave function of the unpaired electron is localized on a silicon atom similar to the dangling-bond defects. The trap of an electron or hole by weak bond, denoted as Si(1)-Si(2), to form $[Si(1)\text{-}Si(2)]^-$ or $[Si(1)\text{-}Si(2)]^+$ might be the origins of the LESR signals. It seems that a microscopic model of the weak Si-Si bond has not been clarified yet. In $Si_3Si(1)\text{-}Si(2)Si_3$ of crystalline silicon, two triangles of basal three silicon atoms are rotated by 120° of each other with Si(1)-Si(2) perpendicular to both basal planes. In some locations of the amorphous network, the Si-Si bond length and the angle connecting two $Si\text{-}Si_3$ units might be substantially deviated from those of crystalline silicon. If the LESR signals are originated from the capture of carriers by weak bonds, the strong localization of the unpaired electron on a silicon atom seems to require a relatively long Si-Si distance in the weak bond and/or a relatively large structural relaxation.

V. SUMMARY

By using the ESEEM method, the weak deuterium hyperfine interaction has been extracted for native dangling bonds, photocreated metastable dangling bonds, and LESR signals in a-Si:D. The distance to the closest deuterium atom, by point-dipole approximation, is 4.2 Å for both native and metastable dangling bonds and is 4.8 Å for LESR signals. If there are two closest deuterium atoms, the distance is 4.8 Å for both native and metastable dangling bonds and is 5.3 Å for LESR signals. The defect creation models proposed to explain the light-induced metastability have been examined based on the distance between the dangling bond and hydrogen atom.

ACKNOWLEDGMENTS

In the initial stages of this work, ESEEM experiments using a-Si:H samples were carried out by using the pulsed ESR spectrometer of Argonne National laboratory. J. I. thanks Professor J. R. Norris and Dr. M. K. Bowman for their kind help in teaching the pulsed ESR techniques.

[1]D. L. Staebler and C. R. Wronski, Appl. Phys. Lett. **32**, 292 (1977).

[2]R. A. Street, D. K. Biegelsen, and J. C. Knights, Phys. Rev. B **24**, 969 (1981).

[3]D. K. Biegelsen and M. Stutzmann, Phys. Rev. B **33**, 3006 (1986).

[4]N. Ishii, M. Kumeda, and T. Shimizu, Jpn. J. Appl. Phys. **21**, L92 (1982).

[5]L. Kevan, in *Time Domain Electron Spin Resonance,* edited by L. Kevan and R. N. Schwartz (Wiley, New York, 1979), pp. 279–341.

[6]W. B. Mims, J. Peisach, and J. L. Davis, J. Chem. Phys. **66**, 5536 (1977).

[7]L. G. Rowan, E. L. Hahn, and W. B. Mims, Phys. Rev. **137**, 61 (1965).

[8]W. B. Mims, Phys. Rev. B **5**, 2409 (1972).

[9]W. B. Mims, in *Electrons Spin Resonance,* edited by S. Geschwind (Plenum, New York, 1972), pp. 263–351.

[10]J. Isoya, M. K. Bowman, J. R. Norris, and J. A. Weil, J. Chem. Phys. **78**, 1735 (1983).

[11]H. Yokomichi and K. Morigaki, Solid State Commun. **63**, 629 (1987).

[12]S. Yamasaki, S. Kuroda, K. Tanaka, and S. Hayashi, Solid State Commun. **50**, 9 (1984).
[13]M. Stutzmann and D. K. Biegelsen, Phys. Rev. B **34**, 3093 (1986).
[14]S. Hayashi, K. Hayamizu, S. Mashima, A. Suzuki, P. J. McElheny, S. Yamasaki, and A. Matsuda, Jpn. J. Appl. Phys. **30**, 1909 (1991).
[15]C. Gemperie, G. Aebli, A. Schweiger, and R. R. Ernst, J. Magn. Reson. **88**, 241 (1990).
[16]J. Isoya, H. Kanda, and Y. Uchida, Phys. Rev. B **42**, 9843 (1990).
[17]K. Tanaka, J. Non-Cryst. Solids, **137&138**, 1 (1992).
[18]S. Yamasaki, M. Kaneiwa, S. Kuroda, H. Okushi, and K. Tanaka, Phys. Rev. B **35**, 6471 (1985).
[19]S. Yamasaki, H. Okushi, A. Matsuda, K. Tanaka, and J. Isoya, Phys. Rev. Lett. **65**, 756 (1990).
[20]M. K. Bowman and R. J. Massoth, in *Electronic Magnetic Resonance of the Solid State,* edited by J. A. Weil (The Canadian Society for Chemistry, Ottawa, 1987), pp. 99–110.
[21]T. Ichikawa, J. Chem. Phys. **83**, 3790 (1985).
[22]W. B. Mims, Phys. Rev. B **6**, 3543 (1972).
[23]M. Stutzmann and D. K. Biegelsen, Phys. Rev. B **40**, 9834 (1989).
[24]H. Yokomichi, I. Hirabayashi, and K. Morigaki, Solid State Commun. **61**, 697 (1987).
[25]M. Stutzmann, W. B. Jackson, and C. C. Tsai, Phys. Rev. B **32**, 23 (1985).
[26]C. Lee, W. D. Ohlsen, and P. C. Taylor, Phys. Rev. B **31**, 100 (1985).
[27]H. Dersch, J. Stuke, and J. Beichler, Appl. Phys. Lett. **38**, 456 (1981).
[28]K. M. Salikhov and Yu. D. Tsvetkov, in *Time Domain Electron Spin Resonance,* edited by L. Kevan and R. N. Schwartz (Wiley, New York, 1979), pp. 231–277.
[29]I. M. Brown, in *Time Domain Electron Spin Resonance,* edited by L. Kevan and R. N. Schwarz (Wiley, New York, 1979), pp. 195–229.
[30]K. Morigaki, Jpn. J. Appl. Phys. **27**, 163 (1988).
[31]D. E. Carlson and C. W. Magee, Appl. Phys. Lett. **33**, 81 (1978).
[32]W. B. Jackson and J. Kakalios, Phys. Rev. B **37**, 1020 (1988).
[33]W. B. Jackson, Phys. Rev. B **41**, 10 257 (1990).
[34]S. T. Pantelides, Phys. Rev. B **36**, 3479 (1987).
[35]D. Adler, Solar Cells **9**, 133 (1983).
[36]H. M. Branz and M. Silver, Phys. Rev. B **42**, 7420 (1990).
[37]R. Fisch and D. C. Licciardello, Phys. Rev. Lett. **41**, 889 (1978).
[38]K. Winer and R. A. Street, Phys. Rev. Lett. **63**, 880 (1989).
[39]R. Jones, Physica B **170**, 181 (1991).
[40]R. Biswas, I. Kwon, and C. M. Soukoulis, Phys. Rev. B **44**, 3403 (1991).
[41]Yu. V. Gorelkinskii and N. N. Nevinnyi, Pis'ma Zh. Techn. Fiz. **13**, 105 (1987) [Sov. Tech. Phys. Lett. **13**, 45 (1987)].
[42]S. Estreicher, Phys. Rev. B **36**, 9122 (1987).
[43]J. Isoya, J. A. Weil, and L. E. Halliburton, J. Chem. Phys. **74**, 5436 (1981).
[44]J. K. Rudra, W. B. Fowler, and F. J. Feigl, Phys. Rev. Lett. **55**, 2614 (1985).
[45]C. G. Van de Walle, P. J. H. Denteneer, Y. Bar-Yam, and S. T. Pantelides, Phys. Rev. B **39**, 10 791 (1989).